The diversity of clinical *Mycobacterium abscessus* isolates in morphology, glycopeptidolipids and infection rates in a macrophage model.

Virginia Pichler[1,3], Lara Dalkilic[1], Ghazaleh Shoaib[1], Tirosh Shapira[1], Leah Rankine-Wilson[1], Yves-Marie Boudehen[3], Joseph Chao[1], Danielle Sexton[1], Miguel Prieto[2], Bradley Quon[2], Elitza Tocheva[1], Laurent Kremer[3], William Hsiao[5], Yossef Av-Gay[1,2]

[1] Department of Microbiology and Immunology, Life Sciences Institute, University of British Columbia, Vancouver, Canada

[2] Department of Medicine, University of British Columbia, Vancouver, Canada

[3] INSERM, IRIM, 34293 Montpellier, France.

[4] Department of Molecular Biology and Biochemistry, Simon Fraser University, Burnaby, Canada

corresponding author: yossi@mailubc.ca

Abstract

Mycobacterium abscessus (Mab) colonies adopt smooth (S) or rough (R) morphotypes, which are linked to the presence or absence of glycopeptidolipids (GPL), respectively. Though clinically relevant, the association between GPL levels, morphotype and pathogenesis are poorly understood. To investigate the degree of correlation between Mab morphology, GPL levels, and infectivity, we generated isolates from Mab-positive sputum samples from cystic fibrosis patients. Isolated strains were categorised based on their morphology, GPL profile, and replication rate in macrophages. Our findings revealed that around 50% of isolates displayed mixed morphologies and GPL analysis confirmed a consistent relationship between GPL content and morphotype was only found in smooth isolates. Across morphotype groups, no differences were observed *in vitro*, yet using a high-content THP-1 cell *ex vivo* infection model, clinical R strains were observed to replicate at higher levels. Moreover, the proportion of infected macrophages was notably higher among clinical R strains compared to their S counterparts at 72 hours post-infection. Clinical variants also infected at significantly higher rates compared to laboratory strains, highlighting the limited translatability of lab strain infection data to clinical contexts. Our study confirmed the general correlation between morphotype and GPL levels in smooth strains yet unveiled more variability within morphotype groups than previously recognised, particularly during intracellular infection. As the rough morphotype is of highest clinical concern, these findings contribute to the expanding knowledge base surrounding Mab infections, offering insights that can steer diagnostic methodologies, and treatment approaches.

Introduction

Non-tuberculous mycobacteria are a class of saprophytic bacteria represented by over 180 species. Ubiquitously found in the environment (soil, water, vegetation), a subset is classified as opportunistic pathogens for their ability to occupy human niches, primarily as pulmonary or soft tissue infections and frequently affecting immunocompromised individuals [1-4]. The most abundant pathogenic species belong to the Mycobacterium avium complex (MAC; *Mycobacterium avium, Mycobacterium intracellulare*) and Mycobacterium abscessus complex (MABSC: *Mycobacterium abscessus abscessus* (Mab), *Mycobacterium abscessus massiliense* (Mma), *Mycobacterium abscessus bolletii* (Mbo)), the latter which remains an ongoing treatment challenge due to its intrinsic resistance to growing incidence of broader antibiotic resistance [5-6].

Mycobacteria follow a similar pathogenesis strategy, primarily infecting hosts via aerosol inhalation where they interact with and are engulfed by the innate immune cells, namely macrophages, where they survive and replicate in phagocytic vesicles [2, 7-8]. This strategy has been well-documented in Mab infections and is associated with the transition of the bacteria from the smooth (S) to rough (R) morphotype [8]. The difference in intracellular behaviour between the two types has been linked to the presence of glycopeptidolipids (GPL) [2]. Cell surface GPL decorate the S morphotype and mask underlying TLR-2 agonists, such a phosphatidyl-myo-inositol dimannoside (PIM2) [9] and lipoproteins [10] and allow for greater initial colonisation in loner phagosomes. Conversely, R morphotypes are associated with a strong immunological response, persistent infections and presence in social phagosomes.

69 The colony morphology of the S morphotype has been described as a uniformly round shape,
70 shiny and luxuriant (Figure 1, left), whereas the R morphotype is often irregular in shape, matte,
71 wrinkled, and textured (Figure 1, right). The characteristics of these opposite morphologies has,
72 indeed, been widely described in the literature, however, to our knowledge no deliberate study
73 has been performed to determine a strict set of criteria for each progressive morphotype
74 between the canonical extremes, represented by the S and R laboratory strains ATCC19977/
75 CIP104536 S/R, denoted as Cip^S and Cip^R throughout. However, rarely do clinical manifestations
76 perfectly mirror their lab counterparts. This is of importance as morphological transition is a
77 marker of infection progression and establishing these criteria will help reduce inter-observer
78 variability when reporting diagnostic results [11]. Furthermore, following consistent
79 morphological plasticity tracking metrics between clinics and research facilities will help build
80 a more robust pool of data to reveal the full extent of the relationship between morphotype
81 and infection persistence and severity. Herein, we describe the isolation, molecular analysis,
82 and intracellular growth of 46 clinical isolates from cystic fibrosis patients, represented by an
83 approximate equal distribution of the S and R morphotypes.
84

Materials and Methods

Clinical Isolates

This study used a total of 46 laboratory-confirmed mycobacterial isolates that were obtained from 19 CF patients in St Pauls Hospital (Vancouver, Canada). Isolates were confirmed through MALDI-TOF MS and 16s rRNA target sequencing and obtained from the B.C. Centre for Disease Control (BCCDC).

Strain separation

BCCDC glycerol stocks were streaked onto Luria Bertani (LB) agar plates and incubated at 37 °C for 4-6 days. Isolates were visually inspected for morphotype composition at high resolution with the Zeiss Axio Zoom V16 microscope according to the categorical descriptors in Table 1. Plates containing heterogenous populations were re-streaked until pure, stable morphotypes were achieved. Single colonies were inoculated in 7H9 Broth (Difco™ Middlebrook) supplemented with 10% (v/v) OADC (0.05% oleic acid, 5% bovine albumin fraction, 2% dextrose, 0.004% catalase, and 0.8% sodium chloride solution) and 0.05% (v/v) Tween 80, termed 7H9OADCT throughout. Glycerol stocks of each step were stored at-80 °C.

Lipid Extraction

Fresh bacterial lawns on LB agar were harvested and pelleted in glass vials by centrifugation at 2,000*g* for 5 min. Polar lipids (GPL) were extracted using the chloroform-methanol method, as described previously [12]. Final extracts were solubilized in 300 µL of chloroform/methanol (2:1 v/v). Lipids were visualised with thin layer chromatography (TLC) by adding 20 µL of sample on a silica gel 60 F254 sheet (Merck) and placed in a chloroform/methanol/water (90:10:1, v/v/v)

solution for migration. An orcinol-sulfuric acid solution (0.2% and 20%, respectively) was sprayed onto the sheet and the plates were lipid profiles revealed using heat. GPL were detected with reference to the control strains (Cip^S, CIP104536T (S) and Cip^R, CIP104536T (R)). Replicates were performed for strains where morphotype categorisation did not align with the TLC results.

Ex-vivo THP-1 macrophage infection model

Construction of an integrative vector expressing a fluorescent marker

Derivative versions of the integrative plasmid pMV306 [13-14] were constructed to allow strong expression of either mScarlet (pMV306-mScarlet, Figure S1) or mWasabi (pMV306-mWasabi) fluorescent proteins with a kanamycin resistant cassette for selection. This plasmid contains pMV306 integrase *attP* as a one-step integration construct. Briefly, the mScarlet or mWasabi coding sequences, placed under the control of the constitutive P left* promoter, were PCR-amplified by Q5® High-Fidelity DNA Polymerase (New England Biolabs) using plasmid L5 attB::Pleft*mScarlet/mWasabi (Addgene plasmids 169410 and 169409, respectively) as DNA templates [15]. Primer pairs, dual forward primer P*: ATCTTTAAATCTAGATGGCCGCGGTACCAGATCTT, mScarlet reverse primer: AGCTGGATCCATGGATTCACTTGTACAGCTCGTCCATGCC, mWasabi reverse primer: AGCTGGATCCATGGATTTACTTGTACAGCTCGTCCATGCC. The linear fragments were purified on agarose gels (NucleoSpin Gel and PCR Clean-up, Macherey- Nagel). Following the manufacturer's instructions, Pro Ligation-Free Cloning Kit (abm®) reactions were performed to insert these linear fragments into the pMV306 previously digested with EcoRV and transformed into *Escherichia coli* (*E. coli*) Stellar TM competent cells (Takara Bio), purified (NucleoSpin

Plasmid, Macherey-Nagel) and verified by DNA sequencing. Plasmids were then electroporated into the *M. abscessus* strains [16-17] and recombinant clones harbouring the constructs inserted at the attL5 insertion site in the glyV tRNA gene were selected for on 7H10 agar supplemented with 0.5% glycerol, 10% OADC, and 50 µg/ml kanamycin (7H10OADCKan).

Bacterial and THP-1 Cell Culturing

Unless otherwise stated, all bacterial strains were transformed with pMV306-mScarlet and routinely grown from stock at 37 °C in 7H9OADCT with 50 µg/ml kanamycin, termed 7H9OADCTKan. THP-1 human monocyte-derived macrophage-like cells (ATCC TIB-202) cells were grown in incomplete RPMI1640 medium (10% FBS, 2% glutamine and 1% non-essential amino acids) at 37 °C with 5% carbon dioxide (CO_2). Cell density was kept between 0.25 and 1 × 10^6 cells/mL for a maximum of three months.

Infection

THP-1 cell suspension at 5 x 10^5 cells/mL in incomplete RPMI1640 was seeded into a 96-well plate at 50,000 cells/well and differentiated into a macrophage-like state over a period of 48 hrs with phorbol12-myristate13-acetate (PMA, 40 ng/mL) at 37 °C with 5% CO_2. Liquid bacterial cultures were grown to mid-log phase in 100 µL per well in a round-bottomed 96-well plate (VWR), centrifuged (5,000*g*, 10 min) and washed once with sterile Dulbecco's phosphate-buffered saline (DPBS, Gibco). Cultures were de-clumped using a 25G blunt needle, transferred to a flat-bottomed 96-well plate (VWR) and OD_{600} was measured (OD_{600} of 1 ≈ 1.13 × 10^9 CFU/mL) using the Varioskan LUX™ microplate reader (Thermo Fisher Scientific). Inoculums of a multiplicity of infection (MOI) of 2 bacteria per macrophage was prepared in incomplete RPMI

and opsonised with 10% non-decomplemented human serum for 30 min at 37 °C, shaking. Differentiated macrophages were washed once with warm DPBS and inoculated with the opsonized bacterial suspensions for three hrs (37 °C, 5% CO_2). Wells were washed twice with DPBS and treated with amikacin (250 µg/mL) for one hr to remove any extracellular bacteria. The amikacin was removed, and wells were washed a final time with DPBS and replaced with 100 µL incomplete RPMI containing 1 µg/mL Hoechst 33342. Plates were incubated for three days at 5% CO_2 at 37 °C. Testing of each strain was performed in technical triplicates.

High-content intracellular growth analysis

Intracellular bacterial growth was monitored using the CellInsight™ CX5 High Content Platform (Thermo Fisher Scientific) using methods previously described by our group [18-19]. Briefly, macrophages were identified and counted through nuclei staining and a mask was created to represent the entire cell, or region of interest (ROI/circle). Red channel fluorescence (569/593 nm) was used to detect bacteria "spots" inside the cellular ROI. These spots were quantified using a variety of measurements including intensity and area using the Thermo Fisher ScientificTM HCS StudioTM Cell Analysis Software. These fluorescent measurements closely correspond with colony-forming units (CFU), as previously validated [20]. Data were potted using GraphPad Prism version 10 (GraphPad Software, Boston, Massachusetts USA, www.graphpad.com). Measurements were captured at multiple time points to monitor replicate rate and bacterial burden. Super-resolution fluorescence light microscopy of the 62S and 62R isolates expressing mScarlet was used to determine morphotype differences after 72 hrs of infection: macrophages were differentiated onto coverslips and infection was carried out as described above, after which, cells were fixed with 4% paraformaldehyde and imaged using Zeiss LSM 900 confocal microscope equipped with an Airyscan 2 detector and a Colibri 5 light

source. Images were collected with a Plan-Apochromat 100x/1.46 oil objective lens and processed using Zen Blue 2.4 software.

Results

Subspecies distribution in CF isolates is predominantly Mab.

19 patients provided 43 unique sputum samples, which were characterised by the BCCDC into 46 clinical isolates, and further categorized in this study, resulting in 75 individually characterised clinical morphotype strains. Subspecies representation was dominated by Mab in categories such as prevalence within patients (n=14, 73.68%), and total clinical isolates (n=38, 82.61%), (Table 2). Mma was the next most prevalent, with the subspecies isolated in 5 of the 19 patients (26.32%). Mbo was isolated from the single sputum sample provided by patient 16. Smooth and rough morphotypes were evenly distributed amongst patients, isolates and strains. 18 patients returned both smooth and rough morphotypes in their sputum samples, and of the 46 BCCDC isolates collected, 27 (58.7%) were further separated into defined both smooth and rough morphotype strains. All BCCDC isolates were correctly identified to the subspecies level.

Colony morphology variation among Mab clinical isolates

Colonies were isolated and subcultured several passages to ensure pure morphotypes were reproducible and stable. Strain colonies were inspected using high resolution zoom microscopy and evaluated for morphotype composition. Colonies most often presented as having uniform margins and smooth texture (smooth, “S”, Figure 1, left) or irregular margins with rough texture throughout (rough, “R”, Figure 1, right) and were classified accordingly.

208 *Visual subcategorization of smooth-like colonies lacks reproducibility.*

209 In addition to the canonical morphotypes, several strains appeared as 'intermediates', along a
210 spectrum between smooth and rough (Figure 2A). A sub-morphotype classification system was
211 initially used to categorise these intermediates, by way of "S-", "S--" and "R-", where S- (Figure
212 2A, *ii-iv*), is more similar to the reference S morphotype (Figure 2A, *i*), than S--, which displays
213 further edge ruffling and is more matte in appearance (Figure 2A, *v-vi*). This categorization
214 strategy became unwieldy, in that there was no definitive characteristic that would separate
215 any one subcategory from their neighbour, and the variability of shape and texture extended
216 beyond these three discrete groupings. In addition, the intermediate colony morphology strains
217 were often not stably reproducible after repeated subculturing. This phenomenon was
218 observed with both intermediate transitioning to smooth, and vice versa over time. We did not
219 observe, nor subsequently explicitly test for morphotype transition to true rough, and later
220 recategorized S- and S-- into the recognised S morphotype class.

221

222 *Some Mab massiliense isolates exhibit density-dependent intermediate morphology.*

223 The putative 'R-' category was defined as individual colonies that consistently carried rough-
224 like features, yet when plated densely, would harbour a central, smooth-like phenotype with
225 rough edges (Figures 2B/C). This phenotype was observed in three patients' unique sputum
226 samples and always belonged to Mma subspecies. 12 (16%) of the 75 strains belonged to Mma.
227 Patient 10 provided two individual samples, one year apart, both only containing Mma (Table
228 2). The first sample yielded a strict R morphotype Mma (70R), while the second sample
229 contained all three morphotypes (S=80S, R=80R, R-=80R-). To further characterise these
230 morphotypes, we next experimentally assessed lipid composition in each strain to determine
231 the presence of GPL.

232

233 *GPL lipid profiles correlate with colony morphology in Mab more than Mma*

234

235 GPL presence was qualitatively assessed using thin layer chromatography (TLC) of lipid extracts.
236 This assay is a simple way to score strains as GPL-positive or-negative by the presence or
237 absence of banding, respectively (Figure 3A). GPL presence and strain morphotype were
238 correctly matched in 100% Mbo and S typed strains and ~97% of Mabs isolates (unmatched
239 n=1, J.R). We recorded five patients who provided samples that contained Mma, which were
240 categorised by BCCDC into seven (15.2%) isolates, that we further classified into 12 distinct
241 strains. As previously stated, three of these samples were identified as putative R- morphotype
242 (67R-, 80R- & 82R-), all of which displayed clear banding in the GLP region of the TLC assay,
243 indicating presence of glycopeptolipids. (Figure 3B-C). Retrospectively, all 12 strains would
244 belong to the smooth morphotype group when considering GPL production.

245

246 The strains were subcultured into both solid and liquid media to ensure purity and lipids re-
247 extracted a total of three times, each instance generating consistent results. Furthermore, the
248 GPL profile to morphotype inconsistency was observed in three Mma strains that were grouped
249 as strict R (70R, 80R & 82R). Mma strains 67, 80 and 82 also possessed strict S morphotypes,
250 showing that Mma has more than one morphology associated with the presence of GPL. This
251 leads us to question whether colony morphology should be supported as a method of
252 morphotyping in Mma strains, and further highlights the inconsistency with this method across
253 all MABSC species. We report the GPL production of Mma strains is not readily determined by
254 visual inspection of colony morphology.

255

256

High-content evaluation reveals intracellular replication is highest among clinical R strains.

A THP-1 macrophage infection model was used to better approximate the behaviour of the separated strains in the context of host. A total of 69 strains, including reference strains, were successfully electrotransformed with the pMV306-mScarlet integrative plasmid containing the red fluorescent protein, which was used to identify intracellular bacteria burden over time. Relative fluorescence from the transformed bacteria were tracked over three days to assess intracellular replication rate. All fluorescence values were normalised to the first time point at 4 hrs to account for any variations in the MOI. Intracellular bacterial burden was evaluated using several parameters, including the relative replication rate of each strain to its respective lab strain, degree of variance between replicates, and the comparison of each morphotype by collapsing data from all strains into S, R, or R- categories.

Growth characteristics of the R- subtype is more closely related to S morphotype than R.

To evaluate each clinical strain relative to its respective lab strain (Cip^R or Cip^S), a multiple comparisons test was performed with a one-way ANOVA on relative fluorescence captured at multiple time points (Figure 4A) and presented as individual, isogenic pairwise and grouped (Figure 4B, C and D, respectively). Cip^S replicated at a rate approximately six-fold greater than Cip^R and was found to be statistically significant ($p<0.001$). Interestingly, clinical strains replicated faster than their cognate lab strain, a characteristic not often reported in clinical strain research. When grouped as isogenic pairs, faster growth was also observed in most R strains compared S strains in the macrophage model (Figures 4C). Indeed, when looking at isogenic strain pairs, nearly all R strains replicated about twice as fast as their S counterparts. Of these, isolates 62, 77, M, A, K and 30 were found to be significantly different. Isolates 77, M and K are sequential collections from Patient 1 and possess both S and R morphotypes. These

281 strains had similar replication rates which were significantly greater ($p<0.01$) than that of the
282 isolate (FR) collected two months prior, indicating a degree of Mab population stability over the
283 subsequent 18 months of infection (Table 2). Isolates 30 and 62 were the bookends of serial
284 samples provided by Patient 5 for this study and also returned significance between the S and
285 R replication rates, though no significant differences between the other isolates of Patient 5
286 were found. The replication rate of *in vitro* growth was also measured by OD_{600} and revealed
287 negligible differences between S and R morphotypes, after 72 hours (Figure 4E).
288
289 To investigate morphotypes as a group, all fluorescence data were collapsed into the discrete
290 S, R and R- clusters to evaluate for broader trends, not otherwise discernible from individual
291 pairs (Figure 4D). All R strains collectively showed a significant two-fold growth to the S strains
292 at 24, 48 and 72 hrs showing intracellular growth is indeed higher in R than S. The putative R-
293 strain closely matched the replicative behaviour of the smooth strains and replicated at a
294 significantly slower rate compared to the bona-fide R group.
295 Considering the faster growth of clinical isolates seen in this study, we wanted to see if variance
296 was affected to a greater extent in clinical strains, and if so, which morphotypes contribute to
297 such variation. We performed a Levene's test to evaluate i) the degree of variance between
298 replicates within a single strain and ii) if any significant differences existed between strains (data
299 not shown). As expected, variance was greatest at 72 hours across all strains, all though no
300 significant differences were observed between strains ($p>0.05$).
301
302
303

Reference strains Cip^S and Cip^R infect macrophages at different rates compared to their clinical counterparts.

The proportion of infected THP-1 macrophages was calculated as a percentage of macrophages with intracellular Mab burden over the total macrophage population per condition (Figure 5A). Cip^S infected a significantly greater proportion of cells compared to the clinical S strains. The clinical R strains (n=22) infected a greater percentage of macrophages, both compared to the lab strain (Cip^R) and the clinical S strains (n=31) at 72 hrs post–infection ($p<0.05$). The high replication rate of Cip^S compared to the clinical S strains complements the higher proportion of macrophages infected. Clinical R strains replicated faster and infected a greater proportion of infected macrophages compared to the Cip^R, whereas inversely, clinical S strains replicated slower and a lesser proportion of infected macrophages compared to Cip^S. This highlights a divergence in pathogenesis of the clinical strains from their associate lab strains. No significant loss in THP-1 survival was seen over the course of infection, either between morphotypes or strains. Further microscopic analysis of the variants revealed that indeed a feature of the R morphotype at later time points is the formation of extensive extracellular cording, exceeding the size of macrophages and hampering phagocytosis as a clearance strategy (Figure 5B/C/D).

Discussion

This study's aim to characterise smooth and rough morphotypes of *M. abscessus* clinical infections was initiated with the separation of strains into the two discrete groups. Strict S colonies are characterised by a uniformly round shape, smooth margin, an absence of interior texture and a beige or brown colour, while strict R colonies are characterised by an irregular shape, rough margins, interior texture and a gray colour (Table 1, Figure 1). After multiple

329 passages of each strain to attain sample purity, it became evident that these two morphotype
330 classes were insufficient to capture the full morphological spectrum.
331
332 *Colony morphology*
333 Subculturing methods aim to isolate a single, pure, stable sample with only one morphotype
334 present. We found some isolates readily conformed to a stable morphotype, but some were
335 highly variable over more than five passages. It is important to note that subcultures with
336 mixed populations never generated both strict S and R morphotypes on the same plate, but
337 rather contained several sub-morphotypes appearing as 'intermediates' between S and R.
338 Initially, these intermediates were classified as 'S+', S++' and 'R-' and fell serially between S and
339 R (i.e., S, S-, S--, R-, R). A subculture isolated from a strict S colony may yield S, S+ and S++ on
340 the same plate, while other strains would only yield more strict S colonies. While the
341 intermediates continued to appear in the subcultures, the inability to successfully isolate
342 consistent sub-morphotypes indicate morphological variations as transient features.
343 Conditions that may have affected colony morphology, such as density, culture age, and media
344 type likely contributed to the observed variability, however, a separate sub-study would need
345 to be performed to properly characterise the full range of factors involved, as has been done
346 on *Pseudomonas aeruginosa* [11]. Despite this limitation, all strains were separated and
347 classified broadly as S and R; all S sub-morphotypes (S+ and S++) fell under the umbrella of S
348 while all strains classified as R adopted the strict morphotype. The 'R-' sub-morphotype, while
349 appearing most like the R morphotype, presented with less texture and brown, rather than
350 gray, in colour (Figure 2C). Additionally, this sub-morphotype forms concentrated, smoothed
351 patches when plated as a lawn (Figure 2B), a feature absent in the strict R morphotype, which
352 is consistently sharply textured even when plated to lawn density. Notably, when reviewing the

353 associated clinical metadata, all strains that possessed the R- sub-morphotype belonged to a
354 congruent subspecies, Mma, and was observed in three of the total seven isolates. While these
355 findings have revealed a common feature of this subspecies' colony behaviour, the R- sub-
356 morphotype was 1) found in mixed populations, often among strict S and R colonies, and 2) not
357 ubiquitous across all seven Mma strains, and therefore cannot serve as a stable speciation proxy
358 for all Mma isolates with microscopy.
359
360 *High-content investigation into MABSC infection dynamics*
361 Clinical *M. abscessus* research has predominantly been performed *in vitro*, which does not
362 adequately reproduce the complexity of the host environment and immunological responses
363 to infection [21]. As the presence of GPL is an important factor in *M. abscessus* pathogenesis,
364 evaluating these bacteria as they interact with macrophages provides a better opportunity to
365 investigate the contributing role of GPL during infection. *For M. abscessus*, a knowledge gap
366 that exists regarding the heterogeneity of a bacterial population and their dynamics during
367 infection may be resolved using high-content analysis. When collapsed by morphotype, we
368 found no significant differences in *in vitro* growth data between groups (Figure 4E). A THP-1
369 macrophage infection model was then used to better approximate behaviour *ex vivo*. We found
370 inverse relationships between clinical and reference morphotyped strains in their ability to
371 infect a population of THP-1 cells over time (Figure 5A). We also noted clinical R strains grew
372 faster than Cip^R in our infection model, a trait that reversed in S morphotypes (Figure 4B).
373 Employing three technical replicates within each experiment was chosen to balance precision
374 and resource efficiency, given that the 54 strains broadly fell into two categories.
375

Traditional CFU/mL assays include a consistent amikacin treatment to control for extracellular growth, thus ensuring that colony quantification post-lysis exclusively comes from the intracellular environment, however, this ignores the process of bacterial escape from macrophage lysis. Mab infection persistence is a combination of two strategies: 1) intracellular survival and apoptosis suppression by the S morphotype, and 2) bacterial escape and extracellular aggregate colonization ('cording') by the R morphotype (Figure 5B/C/D) [1, 8]. By removing the amikacin treatment step over the course of the infection, a truer reflection of infection burden could be seen due to free movement of the bacteria within and between macrophages. Capturing the increase in percent of infected cells demonstrates a degree of bacterial escape and new macrophage infection. Our results show that at 48 and 72 hrs post-infection, the percent of infected macrophages increased in both morphotypes, clinical and lab strains alike. One limitation must be addressed in that our pool of clinical R strains, including most R- strains, was depleted due to difficulty with mScarlet transformation. Some strains underwent several transformation attempts, with additional cell wall perforation methods to enhance DNA uptake [17]. Transformation of mycobacterial species can be especially challenging due to the complex composition of in the cell wall, which often hampers uptake of foreign DNA. The abundance of lipids in the cell wall additionally renders the bacilli hydrophobic, resulting in clumping when grown in media and necessitating the use of de-clumping methods during the preparation of electrocompetent single cells. Rough morphotype strains have been noted as the most challenging to transform and most often form clumps [1]. This was the case for these clinical strains, with ~88% (n=7) of those unsuccessful belonging to the rough morphotype.

399 Nevertheless, the greatest increased observed of infected macrophages were observed in the
400 Cip^{S}, clinical R, clinical S and finally Cip^{R}, reaffirming that the clinical strains do not predictably
401 follow the behaviour of their associated lab strains. Identifying this divergence holds broad
402 implications for our understanding of Mab pathogenesis and persistence. Many studies [1, 7,
403 22-24] have delved into the importance of morphotype distinction, their unique intracellular
404 behaviours, and their strategies to successfully persist in the host environment, but our findings
405 highlight that the features observed in lab strains may be insufficient to fully appreciate the
406 complete diversity and variability found in clinical strains. Most infection studies to date have
407 been completed using reference strains (ATCC199977/CIP104536S/R) alone or fewer than ten
408 clinical isolates, limiting the translatability of the results to authentic clinical contexts [1, 24-
409 27]. This seems to be especially salient as not only do our results show the breadth of
410 behaviour across the strains during infection but show that clinical morphotypes broadly
411 behave inversely to their lab counterparts.
412
413 While the overall trend showed clinical R strains replicating at higher rates than the S strains,
414 large ranges were still observed within each morphotype, with some of the strains more closely
415 matching their associated lab strain. Isogenic strains also varied by fold-difference after 72
416 hours. 83% of R strains replicated faster than their S counterparts, with 75% of the faster
417 growing R strains replicating at 2-3-fold greater than their S strain pair. Of the pairs that saw S
418 strain outgrow R, we highlight the profiles of Patients 1 and 4, where earlier isolates (F and 54,
419 respectively) showed slower replication in the R versus S. However, this trait was reversed in
420 the isogenic pairs from the next patient collection (77 and 57, respectively). In both instances,
421 this was accompanied by the decline in lung function capacity (data not shown). R colony
422 density and shape variability has been noted by Park et al. (2015) [28] in the context of

423 progressive disease, however, the full phenotype spectrum has yet to be elucidated, as is
424 evident by our findings of varied intracellular replication rate and other data describing
425 mutational and transcriptional changes [27, 29-30]. Strains 25S and 50S displayed the greatest
426 amount of intracellular growth within their morphotype at 72 hrs p.i., however, these two
427 strains belong to the subspecies Mma and Mbo, respectively, which could account for notable
428 difference.

429

430 The higher proportion of infected cells seen in clinical R morphotype may be due to bacterial
431 escape and subsequent increased macrophage TLR receptor engagement to
432 immunostimulatory surface molecules, such as PIMs and lipoproteins, that are otherwise
433 masked by GPL in the S morphotype [31]. The stable cell survival between both morphotypes,
434 and increase in infected cells over time do not support the supposition of macrophage
435 apoptosis and bacterial release. The increase in infected macrophages without cell lysis may
436 attributed in part, to the stimulation of tunneling nanotubes (TNTs), membrane channels that
437 connect cells as a rescue function during stress for the transfer of essential cellular
438 components, such as mitochondria [32]. TNT-like structures have been shown to play a role in
439 dissemination of several intracellular pathogens and have been observed in other
440 mycobacteria, including *M. marinum* and *M. bovis* BCG [33-34].

441

442 ## Conclusions

443

444 This study aimed to further characterise the morphological variations and behaviours exhibited
445 within clinical *M. abscessus* infections. We revealed a relationship between clinical and
446 reference strain behaviour in both phenotypic morphotype and intracellular behaviour.

We highlight the complexity of working with clinical isolates, particularly with the heterogeneity of intracellular replication observed even within each morphotype group. By evaluating strain pairs in an intracellular model, we observed R strain enhanced growth rate compared with S, which likely contributed in part to R strain variability. Together, these data encourage the development of specific R and S strain methodologies when assessing host-pathogen relationships.

Considering these findings, we suggested that the existing S-to-R framework should be considered more as a reference point rather than an absolute standard. This framework can serve as a foundation to drive deeper comprehension of infection progression, as well as the development of virulence and resistance mechanisms. Embracing a more flexible approach to morphotype classification could facilitate a more nuanced understanding of *M. abscessus* infections and aid in the development of more effective therapeutic interventions.

Conflicts of interest

None declared.

Funding

Funding for this research was provided by the Friedman Award for Scholars in Health (UBC, awarded to V. Pichler), Cystic Fibrosis Canada (AWD-021084, awarded to Y. Av-Gay), and the French National Research Agency ANR grants 19-CE15-0012-01 (SUNLIVE, awarded to L. Kremer).

Acknowledgments

The authors wish to thank M. Ko, F. Roquet-Baneres, W. Daher for technical assistance and helpful discussions.

476 ## References

477 1. Roux AL, Viljoen A, Bah A, Simeone R, Bernut A, Laencina L, Deramaudt T, Rottman M,
478 Gaillard JL, Majlessi L, Brosch R. The distinct fate of smooth and rough Mycobacterium
479 abscessus variants inside macrophages. Open biology. 2016 Nov 1;6(11):160185.
480 2. Johansen MD, Herrmann JL, Kremer L. Non-tuberculous mycobacteria and the rise of
481 Mycobacterium abscessus. Nature Reviews Microbiology. 2020 Jul;18(7):392-407.
482 3. Lee MR, Sheng WH, Hung CC, Yu CJ, Lee LN, Hsueh PR. Mycobacterium abscessus
483 complex infections in humans. Emerging infectious diseases. 2015 Sep;21(9):1638.
484 4. Abdelaal HF, Chan ED, Young L, Baldwin SL, Coler RN. Mycobacterium abscessus: it's
485 complex. Microorganisms. 2022 Jul 19;10(7):145.
486 5. Clary G, Sasindran SJ, Nesbitt N, Mason L, Cole S, Azad A, McCoy K, Schlesinger LS, Hall-
487 Stoodley L. Mycobacterium abscessus smooth and rough morphotypes form
488 antimicrobial-tolerant biofilm phenotypes but are killed by acetic acid. Antimicrobial
489 agents and chemotherapy. 2018 Mar;62(3):10-128.
490 6. Phelps GA, Cheramie MN, Fernando DM, Selchow P, Meyer CJ, Waidyarachchi SL,
491 Dharuman S, Liu J, Meuli M, Molin MD, Killam BY. Development of 2nd generation
492 aminomethyl spectinomycins that overcome native efflux in Mycobacterium abscessus.
493 Proceedings of the National Academy of Sciences. 2024 Jan 9;121(2):e2314101120.
494 7. Bernut A, Herrmann JL, Kissa K, Dubremetz JF, Gaillard JL, Lutfalla G, Kremer L.
495 Mycobacterium abscessus cording prevents phagocytosis and promotes abscess
496 formation. Proceedings of the National Academy of Sciences. 2014 Mar
497 11;111(10):E943-52.
498 8. Gutiérrez AV, Viljoen A, Ghigo E, Herrmann JL, Kremer L. Glycopeptidolipids, a double-
499 edged sword of the Mycobacterium abscessus complex. Frontiers in microbiology. 2018
500 Jun 5;9:1145.
501 9. Rhoades ER, Archambault AS, Greendyke R, Hsu FF, Streeter C, Byrd TF. Mycobacterium
502 abscessus glycopeptidolipids mask underlying cell wall phosphatidyl-myo-inositol
503 mannosides blocking induction of human macrophage TNF-α by preventing interaction
504 with TLR2. The Journal of Immunology. 2009 Aug 1;183(3):1997-2007.
505 10. Roux AL, Ray A, Pawlik A, Medjahed H, Etienne G, Rottman M, Catherinot E, Coppée JY,
506 Chaoui K, Monsarrat B, Toubert A. Overexpression of proinflammatory TLR-2-signalling

lipoproteins in hypervirulent mycobacterial variants. Cellular microbiology. 2011 May;13(5):692-704.

11. Sousa AM, Machado I, Nicolau A, Pereira MO. Improvements on colony morphology identification towards bacterial profiling. Journal of microbiological methods. 2013 Dec 1;95(3):327-35.
12. Daher W, Leclercq LD, Johansen MD, Hamela C, Karam J, Trivelli X, Nigou J, Guerardel Y, Kremer L. Glycopeptidolipid glycosylation controls surface properties and pathogenicity in Mycobacterium abscessus. Cell chemical biology. 2022 May 19;29(5):910-24.
13. Stover CK, de la Cruz VF, Fuerst TR, Burlein JE, Benson LA, Bennett LT, Bansal GP, Young JF, Lee MH, Hatfull GF, et al. New use of BCG for recombinant vaccines. Nature. 1991 Jun 6;351(6326):456-60. doi: 10.1038/351456a0.
14. Huff J, Czyz A, Landick R, Niederweis M. Taking phage integration to the next level as a genetic tool for mycobacteria. Gene. 2010 Nov 15;468(1-2):8-19.
15. Kolbe K, Bell AC, Prosser GA, Assmann M, Yang HJ, Forbes HE, Gallucci S, Mayer-Barber KD, Boshoff HI, Barry Iii CE Development and Optimization of Chromosomally-Integrated Fluorescent Mycobacterium tuberculosis Reporter Constructs.. Front Microbiol. 2020 Dec 9;11:591866. doi: 10.3389/fmicb.2020.591866. eCollection 2020. 10.3389/fmicb.2020.591866 PubMed 33362741
16. Medjahed H, Singh AK. Genetic manipulation of Mycobacterium abscessus. Current Protocols in Microbiology. 2010 Aug;18(1):10D-2.
17. Campo-Pérez V, del Mar Cendra M, Julián E, Torrents E. Easily applicable modifications to electroporation conditions improve the transformation efficiency rates for rough morphotypes of fast-growing mycobacteria. New biotechnology. 2021 Jul 25;63:10-8.
18. Rankine-Wilson L, Rens C, Sahile HA, Av-Gay Y. Mycobacterium tuberculosis Infection of THP-1 Cells: A Model for High Content Analysis of Intracellular Growth and Drug Susceptibility. Methods in Molecular Biology (Clifton, NJ). 2022 Jan 1;2427:73-82.
19. Richter A, Strauch A, Chao J, Ko M, Av-Gay Y. Screening of preselected libraries targeting Mycobacterium abscessus for drug discovery. Antimicrobial Agents and Chemotherapy. 2018 Sep;62(9):10-128.
20. Richter A, Shapira T, Av-Gay Y. THP-1 and dictyostelium infection models for screening and characterization of anti-mycobacterium abscessus hit compounds. Antimicrobial Agents and Chemotherapy. 2019 Dec 20;64(1):10-128.

21. Victoria L, Gupta A, Gómez JL, Robledo J. Mycobacterium abscessus complex: a review of recent developments in an emerging pathogen. Frontiers in cellular and infection microbiology. 2021 Apr 26;11:659997.
22. Tsai SH, Lai HC, Hu ST. Subinhibitory doses of aminoglycoside antibiotics induce changes in the phenotype of Mycobacterium abscessus. Antimicrobial agents and chemotherapy. 2015 Oct;59(10):6161-9.
23. Byrd TF, Lyons CR. Preliminary characterization of a Mycobacterium abscessus mutant in human and murine models of infection. Infection and immunity. 1999 Sep 1;67(9):4700-7.
24. Kam JY, Hortle E, Krogman E, Warner SE, Wright K, Luo K, Cheng T, Manuneedhi Cholan P, Kikuchi K, Triccas JA, Britton WJ. Rough and smooth variants of Mycobacterium abscessus are differentially controlled by host immunity during chronic infection of adult zebrafish. Nature Communications. 2022 Feb 17;13(1):952.
25. Ordway D, Henao-Tamayo M, Smith E, Shanley C, Harton M, Troudt J, Bai X, Basaraba RJ, Orme IM, Chan ED. Animal model of Mycobacterium abscessus lung infection. Journal of Leucocyte Biology. 2008 Jun;83(6):1502-11.
26. Bernut A, Dupont C, Sahuquet A, Herrmann JL, Lutfalla G, Kremer L. Deciphering and imaging pathogenesis and cording of Mycobacterium abscessus in zebrafish embryos. JoVE (Journal of Visualized Experiments). 2015 Sep 9(103):e53130.
27. Pawlik A, Garnier G, Orgeur M, Tong P, Lohan A, Le Chevalier F, Sapriel G, Roux AL, Conlon K, Honoré N, Dillies MA. Identification and characterization of the genetic changes responsible for the characteristic smooth-to-rough morphotype alterations of clinically persistent Mycobacterium abscessus. Molecular microbiology. 2013 Nov;90(3):612-29.
28. Park IK, Hsu AP, Tettelin H, Shallom SJ, Drake SK, Ding L, Wu UI, Adamo N, Prevots DR, Olivier KN, Holland SM. Clonal diversification and changes in lipid traits and colony morphology in Mycobacterium abscessus clinical isolates. Journal of clinical microbiology. 2015 Nov;53(11):3438-47.
29. Chhotaray C, Wang S, Tan Y, Ali A, Shehroz M, Fang C, Liu Y, Lu Z, Cai X, Hameed HA, Islam MM. Comparative analysis of whole-genome and methylome profiles of a smooth and a rough Mycobacterium abscessus clinical strain. G3: Genes, Genomes, Genetics. 2020 Jan 1;10(1):13-22.

30. Li B, Ye M, Zhao L, Guo Q, Chen J, Xu B, Zhan M, Zhang Y, Zhang Z, Chu H. Glycopeptidolipid genotype correlates with the severity of Mycobacterium abscessus lung disease. The Journal of Infectious Diseases. 2020 Mar 16;221(Supplement_2):S257-62.
31. Parmar S, Tocheva EI. The cell envelope of Mycobacterium abscessus and its role in pathogenesis. PLoS Pathogens. 2023 May 18;19(5):e1011318.
32. Mittal R, Karhu E, Wang JS, Delgado S, Zukerman R, Mittal J, Jhaveri VM. Cell communication by tunneling nanotubes: Implications in disease and therapeutic applications. Journal of cellular physiology. 2019 Feb;234(2):1130-46.
33. Marzo L, Gousset K, Zurzolo C. Multifaceted roles of tunneling nanotubes in intercellular communication. Frontiers in physiology. 2012 Apr 10;3:72.
34. Tiwari V, Koganti R, Russell G, Sharma A, Shukla D. Role of tunneling nanotubes in viral infection, neurodegenerative disease, and cancer. Frontiers in Immunology. 2021 Jun 14;12:680891.

603 Figure legends

604

605 **Figure 1.** Characteristic two morphotypes of M. abscessus. A. smooth (left) and rough (right).
606 The smooth (S) morphotype is shiny and luxuriant with a uniformly round shape; the rough (R)
607 morphotype is matte, wrinkled, and textured with an irregular in shape.

608

609 **Figure 2.** A. M. abscessus morphology variability. Several 'intermediates' colony subtypes (*ii-vii*)
610 appear among clinical strains and deviate from the strict smooth or rough morphotype,
611 represented by the first and last images in the series. B. The putative 'R-' phenotype appears
612 rough in individual colonies but adopts a smooth-like characteristic when plated densely (white
613 arrow). C. Putative 'R-' colony with rugged edges, smoother centre and brown colour.

614

615 **Figure 3**. Glycopeptidolipid profiles. A. Cell surface glycopeptidolipids (GPL) are shown in the
616 upper banding of the TLC, with DAT, TMM, and PIM lipids making up the lower bands. GPL
617 present in isolates F and M are smooth morphotypes and match the associated lab strain (Cip^S);
618 isolate G is a rough morphotype and matches its associated lab strain (Cip^R). GPL will be present
619 on TLC of mixed morphology isolates, as the rough morphotype is confirmed only by the
620 absence of GPL. Mixed isolates should first be subcultured into pure morphotypes before polar
621 lipid extraction and visualised on a TLC. B. TLC of GPL composition in several clinical isolates,
622 already separated by morphotype. 70R and 80R/R- were morphologically categorised as rough
623 strains yet present with GPL banding. Isolates 70 and 80 are serial collections from the same
624 patient and belong to the subspecies Mma, which may indicate morphological features unique
625 to the subspecies that differ from Mab. C. Repeat extraction and TLC of isolates 70 and 80 to
626 confirm GPL presence.

627

628 **Figure 4.** Clinical strain growth rates. A. Relative fluorescence intensity of intracellular M.
629 abscessus clinical strains at 24, 48, and 72 hrs, as normalised to the 4-hr starting time point. All
630 strains were prepared to the same starting inoculum concentration and left to infect THP-1
631 macrophages for 3 hrs in triplicate, followed by a 1-hr 250 µg/mL amikacin treatment to clear
632 any remaining extracellular bacteria. Lower fluorescence intensity is represented in pale green
633 and high intensity in dark blue. Broadly, S strains (left of plot) replicate as a slower rate than the
634 R strains (right of plot), with the greater divergence appearing at 48 and 72 hrs. Reference

strains Cip^S and Cip^R adopt the inverse replication rate to their clinical counterparts. Overall, there is greater replication rate variability among the R strains. Isolate 82R-, which was classified as an 'intermediate' morphotype clusters more closely with the S strains. Other notable outliers, including 25S and 50S belong to the subspecies Mbo and Mma, respectively. B. Intracellular bacterial growth of all isolates at 72 hrs post-infection, grouped by variant. C. Intracellular bacterial growth of isogenic pairs at 72 hrs post-infection. A one-way ANOVA showed statistical significance between the lab strains, Cip^S and Cip^R ($p = 0.0016$), and additionally between the isogenic pairs of 62 ($p = 0.009$), 77 ($p = 0.038$) and M ($p = 0.0052$). D. All strains collapsed into morphotype group over 72 hrs. There were no significance differences in rate between groups (S, n=37; R, n=35; R-, n=3). E. Clinical isolate intracellular bacterial replication measured through fluorescence intensity, collapsed by morphotype (S, n=31; R n=22; R-, n=1). R strains replicate at a rate approximately 2-fold higher than that of the S strains and differ significantly at 24, 48 and 72 hrs p.i. The 'R-' intermediate strain (n =1) significantly differed from the R strains, but not the S, indicating it clusters with the intracellular replication behaviour of the S morphotype.

Figure 5. Infection burden. A. Percent of THP-1 macrophage infection by morphotype, clinical and lab strain. The proportion of infected THP-1 macrophages was significantly greater among the R clinical strains compared to their S counterparts at 72 hrs post-infection. Clinical morphotype groups also infected a greater percentage of THP-1 macrophages compared to their associated lab strains. B. High content fluorescent microscopy (CellInsightTM CX5 High Content platform, Thermo Fisher Scientific) image of isolate 62R at 72 hrs post-infection. Macrophage nuclei are stained blue and Mab is expressing mScarlet, with notable cording forming extracellularly. C/D. Super-resolution fluorescence light microscopy of 62R (D) and 62S (E) isolates, 72 hrs post-infection. The R morphotype is found on the surface of macrophages (outlined with white dashed line) with distinct 'cording' appearance indicative of cell aggregates too large for clearance by phagocytosis.

Figure S1. Construct map of the pMV306-mScarlet plasmid.

	Cip^S	Cip^R
Appearance	Shiny	Matte, textured
Colour	Brown	Gray
Margin	Uniform	Irregular
Glycopeptidolipid	Present	Absent
Infection stage	Colonising	Persistent
Antibiotic resistance	Low	High

Table 1. Canonical features of smooth (Cip^S) and rough (Cip^R) morphotypes.

Patient (n=19)	Isolate (n=46)	Isolation Date (YYYY-MM-DD)	Species	Morphotypes		
				S (n=37)	R (n=35)	'R-' (n=3)
1	10	2013-03-07	Mab	●		
	F	2018-06-08	Mab	●	●	
	77	2018-08-15	Mab	●	●	
	M	2019-01-17	Mab	●	●	
	K	2020-02-03	Mab	●	●	
	J	2021-05-05	Mab	●	●	
	G	2021-05-05	Mab		●	
2	8	2013-06-24	Mab	●	●	
	26	2014-03-09	Mab		●	
	45	2015-07-12	Mab	●	●	
	49	2016-03-18	Mab	●	●	
	D	2016-10-05	Mab		●	
	I	2017-06-09	Mab		●	
3	79	2018-07-09	Mab	●		
	76	2018-08-13	Mab	●		
	C	2018-08-13	Mma	●		
	B	2018-12-01	Mab	●		
4	54	2016-06-28	Mab	●	●	
	57	2016-10-21	Mab	●	●	

	L	2019-05-09	Mab	•	•	
	A	2019-09-19	Mab	•	•	
5	30	2014-12-01	Mab	•	•	
	43	2015-05-10	Mab		•	
	52	2016-06-20	Mab	•	•	
	62	2017-01-19	Mab	•	•	
6	E	2018-10-29	Mab	•	•	
	81	2018-10-29	Mab	•	•	
7	50	2016-03-31	Mma	•		
	82	2018-05-12	Mma	•	•	•
8	29	2014-11-20	Mab	•		
	42	2015-09-21	Mab	•	•	
9	27	2014-02-10	Mab	•		
	72	2018-10-01	Mab	•	•	
10	70	2017-10-15	Mma		•	
	80	2018-09-27	Mma	•	•	•
11	22	2014-04-30	Mab	•		
	N	2019-01-23	Mab		•	
12	6	2013-04-18	Mab	•	•	
13	7	2013-05-28	Mab		•	
	15	2013-11-29	Mab	•	•	
14	16	2013-05-12	Mma	•		
15	23	2014-01-06	Mab		•	
16	25	2014-03-09	Mbo	•	•	
17	67	2017-09-07	Mma	•		•
18	75	2018-08-09	Mab	•	•	
19	H	2019-05-22	Mab	•	•	

Table 2. Patient sample isolation dates, species and morphotype categorisation.

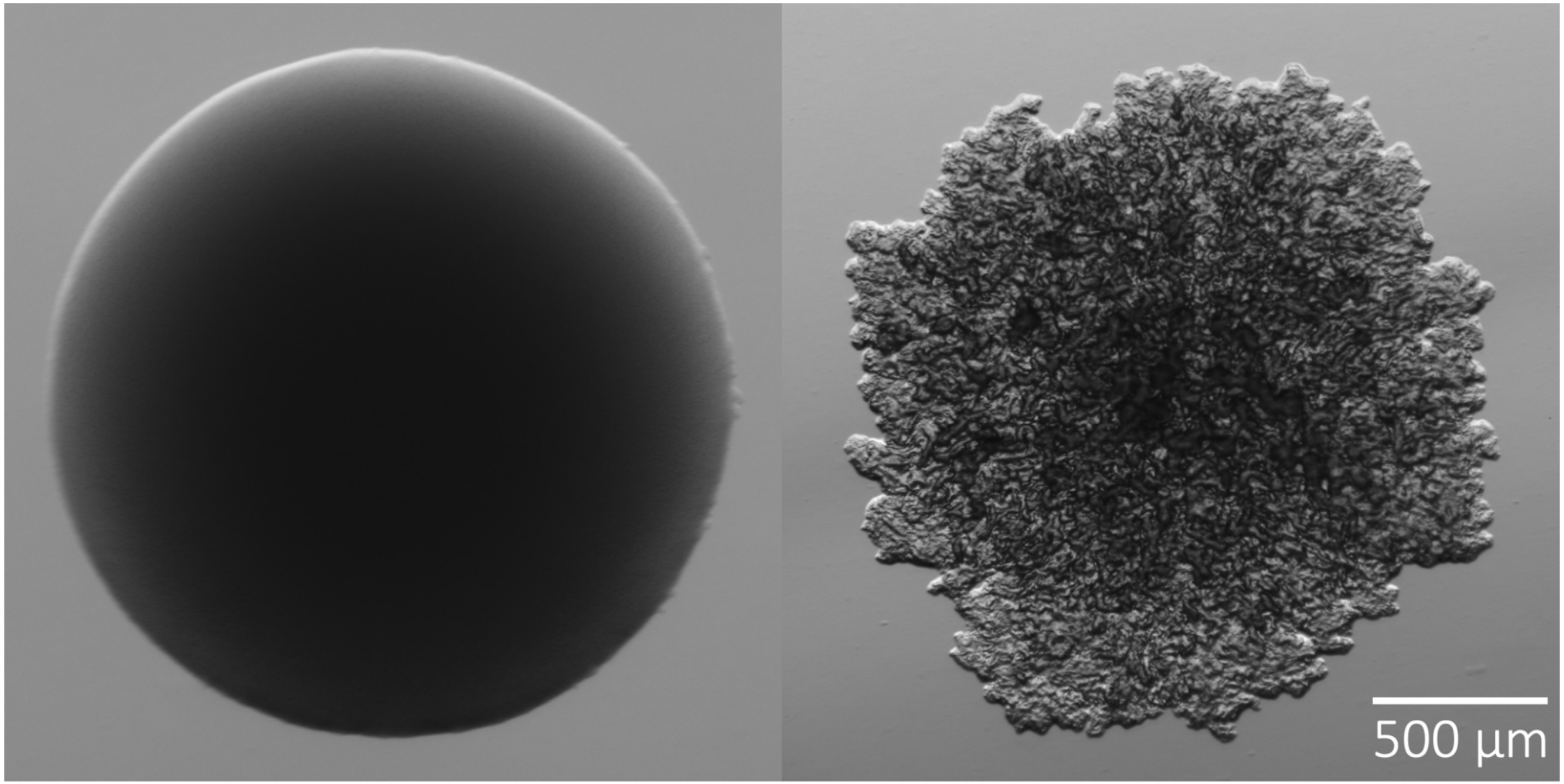

Figure 1

A

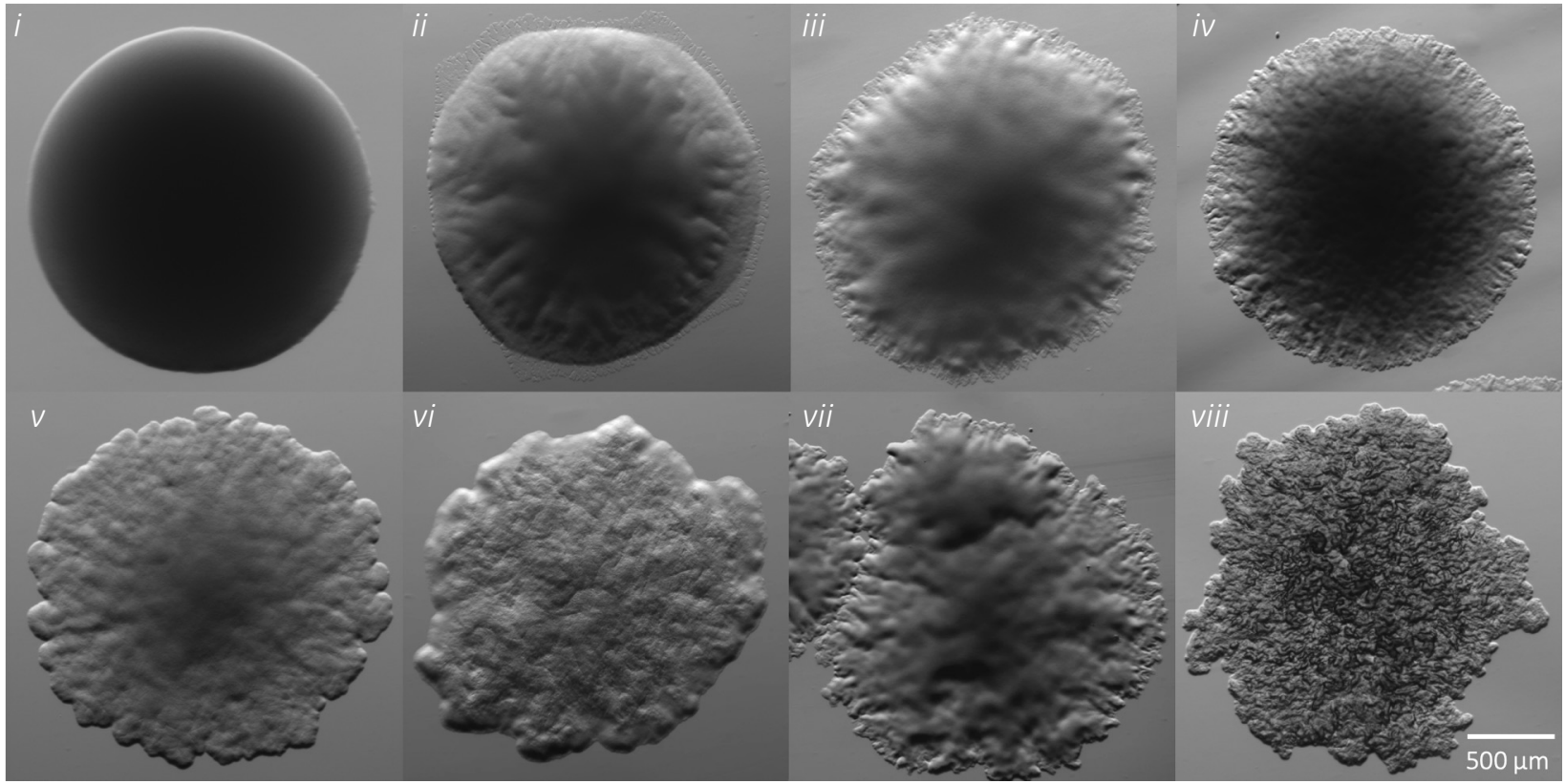

B

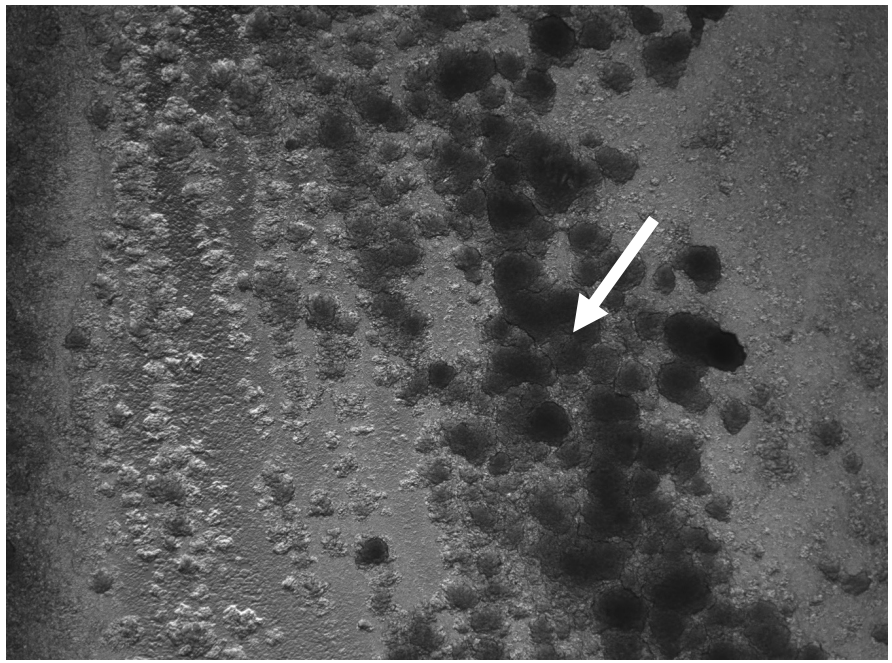

C

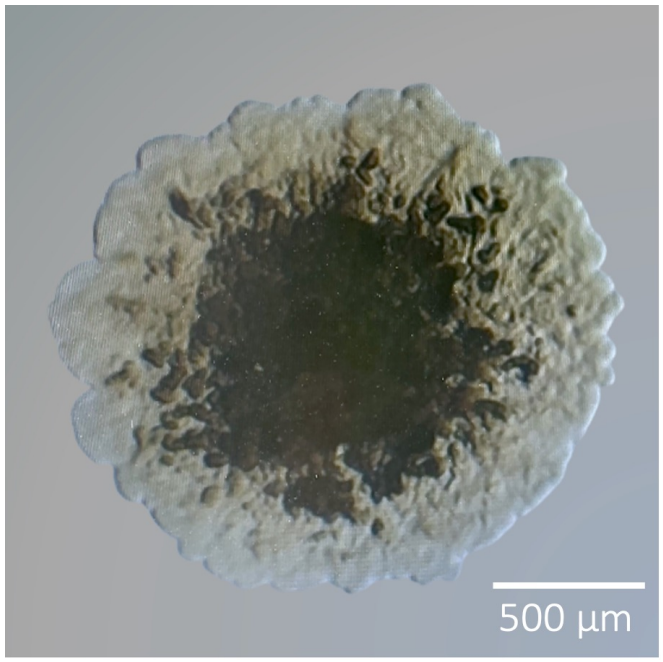

Figure 2

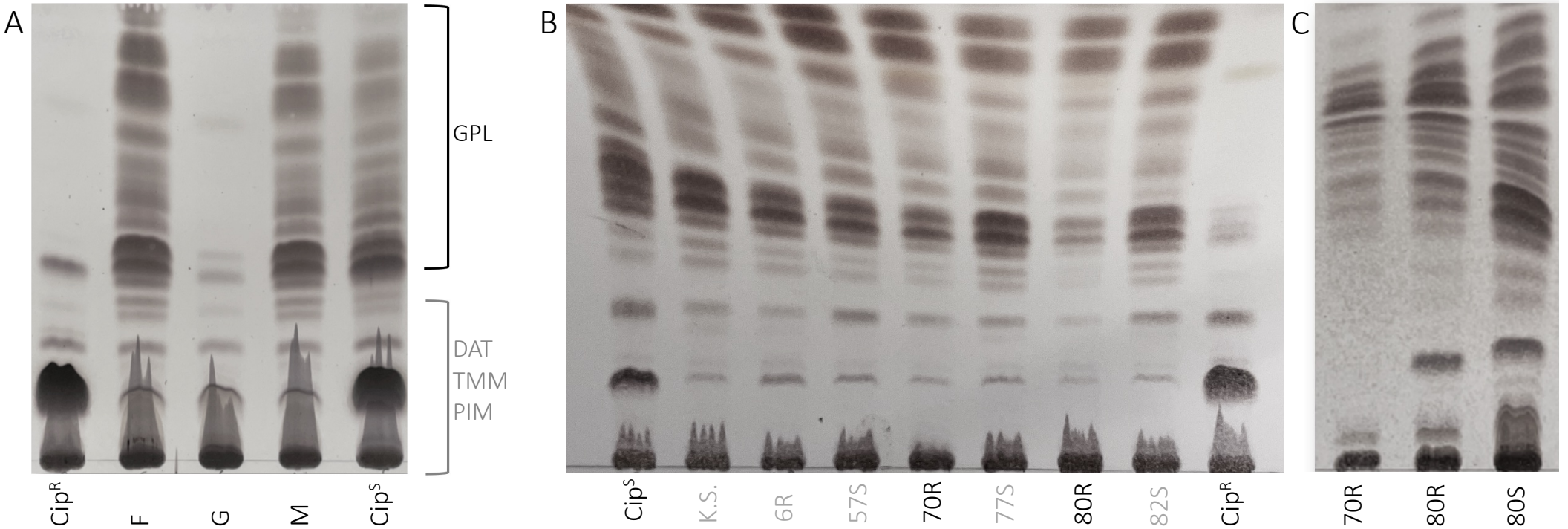
A
GPL
DAT
TMM
PIM
Cip^R
F
G
M
Cip^S
B
Cip^S
K.S.
6R
57S
70R
77S
80R
82S
Cip^R
C
70R
80R
80S

Figure 3

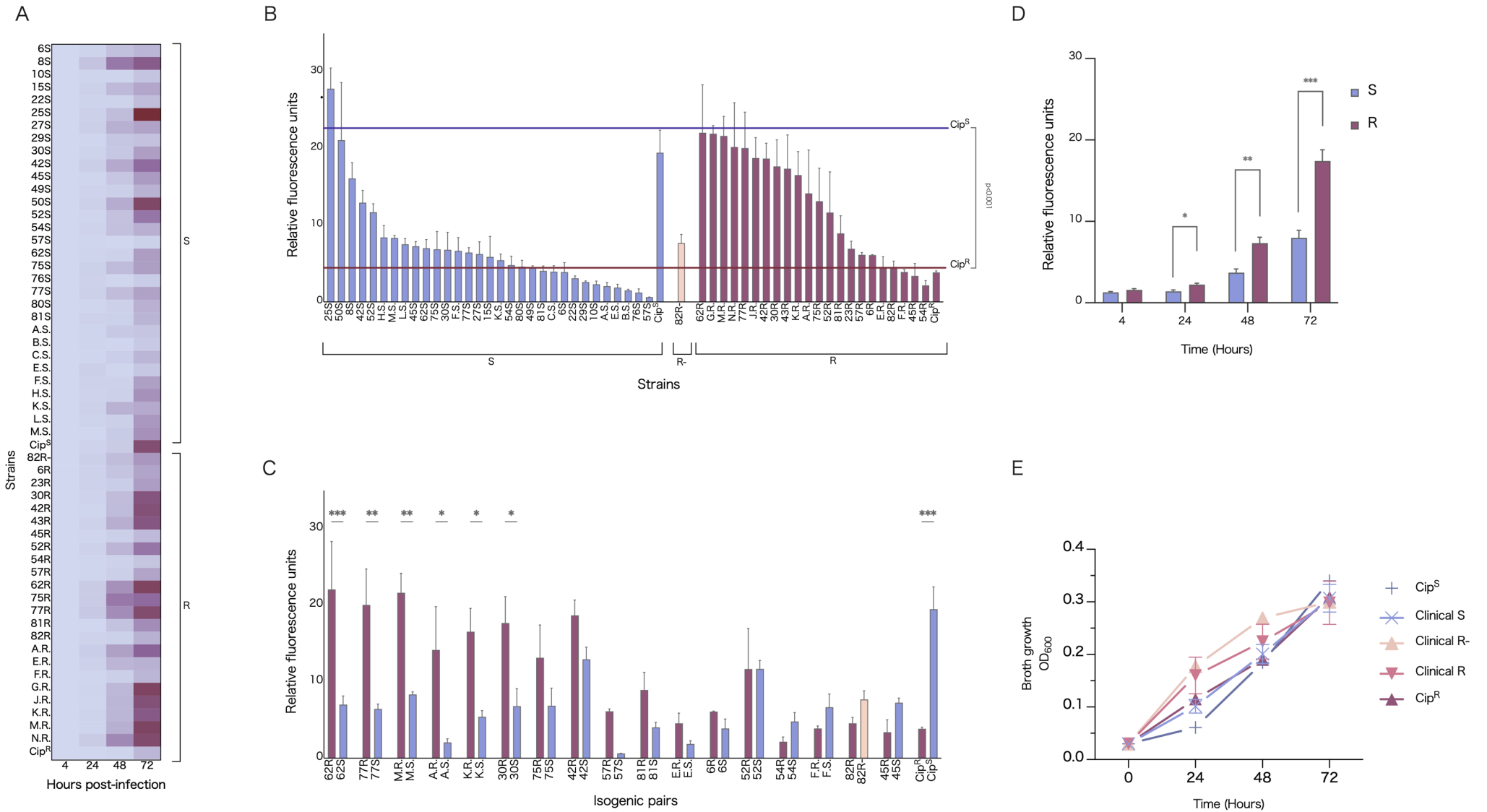
A
Strains
Hours post-infection
4
24
48
72
S
R
B
Relative fluorescence units
Strains
S
R-
R
p<0.001
C
Relative fluorescence units
Isogenic pairs
D
Relative fluorescence units
Time (Hours)
S
R
E
Broth growth
OD600
Time (Hours)
Clinical S
Clinical R-
Clinical R

Figure 4

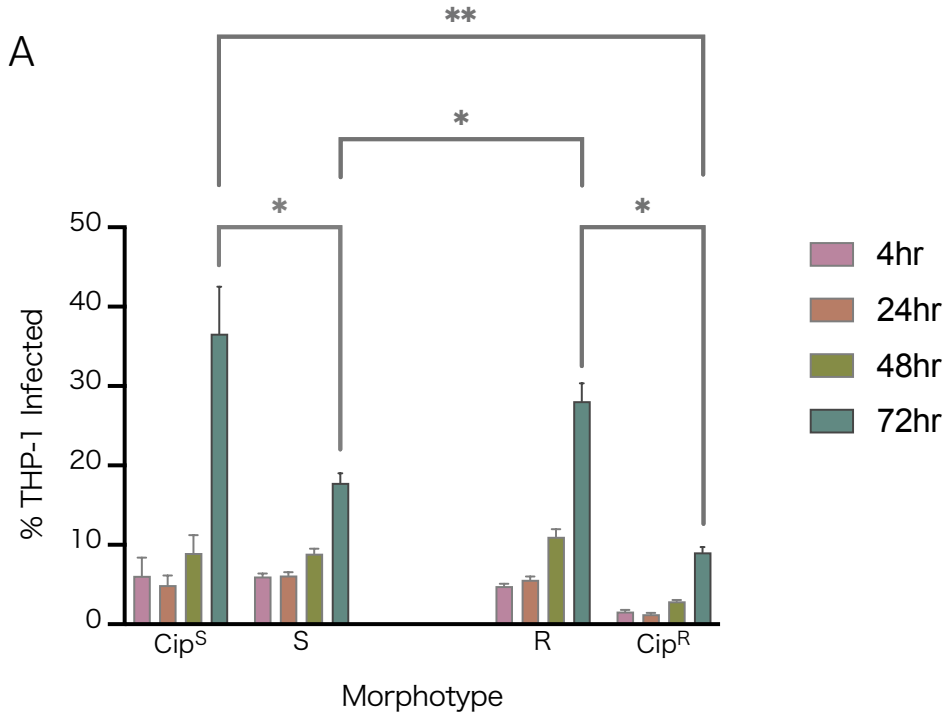
A
**
*
*
*
50
40
30
20
10
0
% THP-1 Infected
Cip^S
S
R
Cip^R
Morphotype
4hr
24hr
48hr
72hr

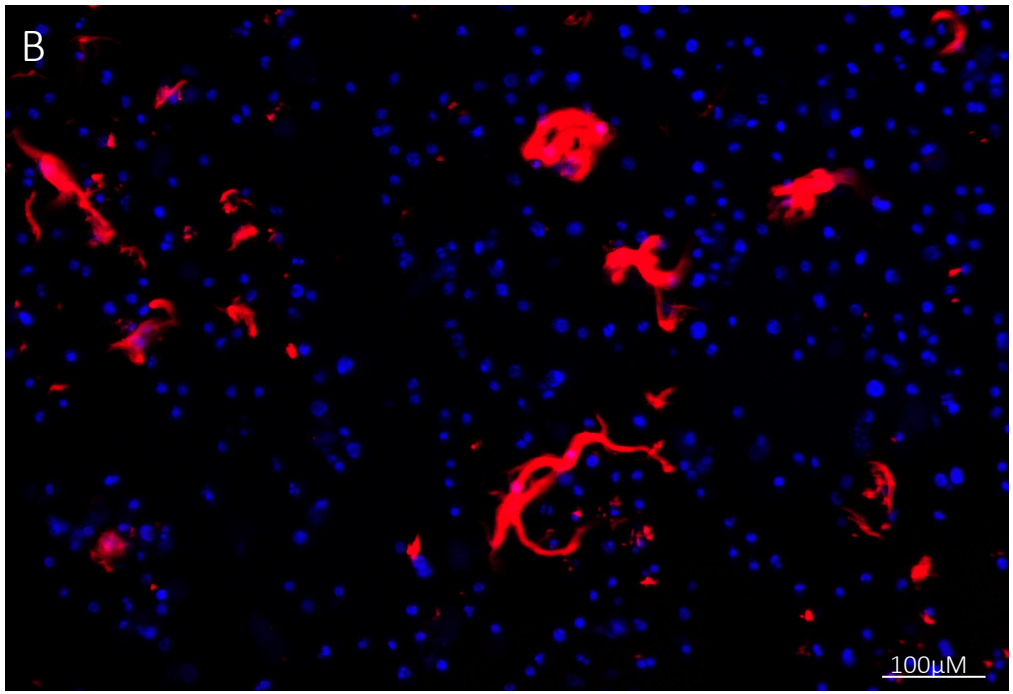
B
100µM

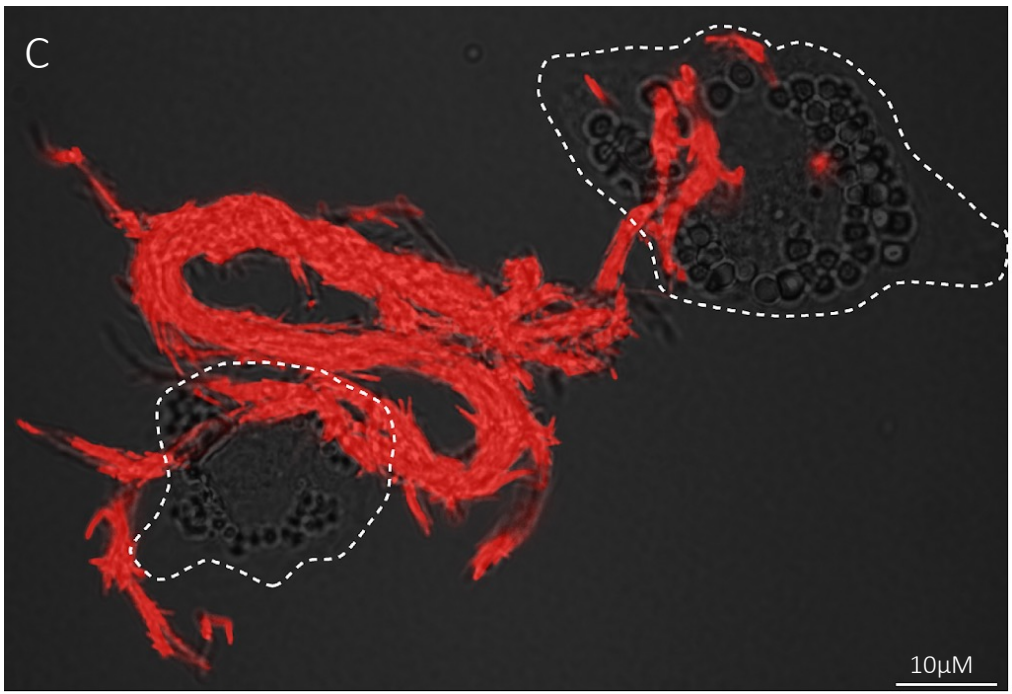
C
10µM

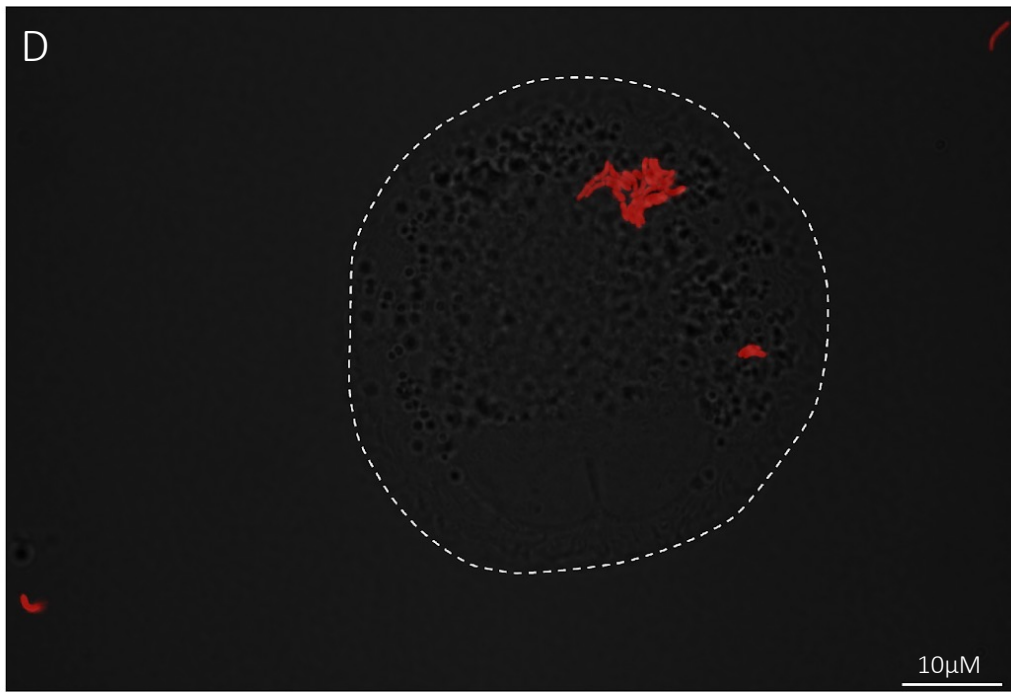
D
10µM

Figure 5

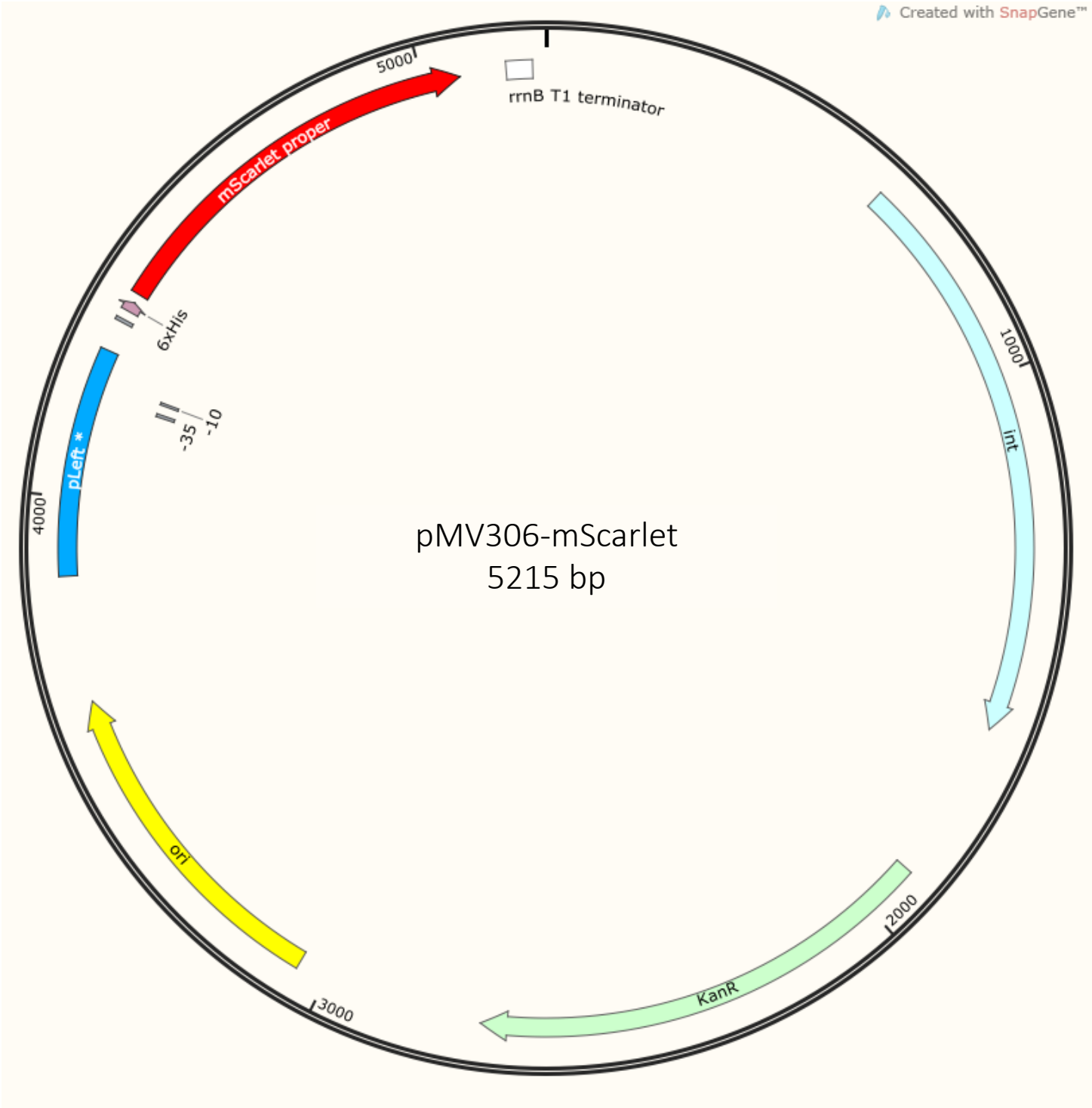
Created with SnapGene™
pMV306-mScarlet
5215 bp
5000
rrnB T1 terminator
mScarlet proper
6xHis
-35
-10
pLeft *
4000
1000
int
ori
3000
KanR
2000

Figure S1